Clay Minerals (2002) **37**, 473–486

Structural insights from the study of Cs-exchanged smectites submitted to wetting-and-drying cycles

J. CUADROS*

Department of Mineralogy, The Natural History Museum, Cromwell Road, London SW7 5BD, UK

(*Received 15 September 2001; revised 10 December 2001*)

ABSTRACT: Six smectites of different tetrahedral and octahedral compositions (SAz-1, Chambers, Belle Fourche, two subsamples of nontronite 33B and SWy-1) were Cs-exchanged and submitted to 70 wetting-and-drying cycles. X-ray diffraction (XRD) of oriented and glycolated mounts of the resultant material showed non-expandable layer proportions ranging from 15 to 60%. They were also analysed by powder XRD at 200°C in vacuum. These patterns showed that 15–40% of the layers were not rotated relative to each other and the rest were randomly rotated (no rotations of the 60° and 120° types). All layers had a *d*-spacing of 11 Å, corresponding to collapsed layers with Cs in the cavities created by the hexagonal rings of the tetrahedral sheets. Analysis of the number of cavities available in relation to the layer rotation shows that the rotation angle must be close to 30° or its multiples 90, 150, 210, 270 and 330°. X-ray diffraction and thermal analysis detected the same proportion of *cis*- and *trans*-vacant sites in the smectites. The ideal *b* dimensions of the tetrahedral and octahedral sheets (the sheets are considered independently, without deformation) were calculated for the samples used in this work and for others from the literature, using the tetrahedral and octahedral compositions. These ideal *b* dimensions have a strong positive correlation. The *cis*/*trans*-vacant character of the smectites is related to the relative lateral dimensions of the ideal tetrahedral and octahedral sheets. A possible explanation of this fact is offered, in which the different configurations of hydroxyls and oxide ions in *cis*- and *trans*-vacant structures can affect octahedral-sheet dimension.

KEYWORDS: caesium exchange, *cis-trans* occupancy, layer rotation, octahedral-tetrahedral fit, smectite, wetting-and-drying cycles.

Structural analysis of smectite is a difficult task, made complex by the existence of variable tilt angles between layers, layer rotation or displacement, variable occupation of *cis* (M2) and *trans* (M1) octahedral sites, variable composition of the interlayer and octahedral sheet, and variable cation ordering within the octahedral sheet. Computer simulations of X-ray diffraction (XRD) patterns allow an assessment of the structural characteristics of smectite. This method is helped significantly if the smectite is exchanged with large anhydrous cations (Cs, K) that minimize the number of stacking defects, and the ordering effect of Cs or K exchange is improved by submitting the exchanged specimen to wetting-and-drying cycles (Drits *et al.*, 1984; Tchoubar, 1985).

Recent studies of mixed-layer illite-smectite have prompted analysis of the compositional and structural features indicated above, using XRD modelling and other techniques such as infrared (IR), thermal analysis, nuclear magnetic resonance (NMR), Mössbauer and extended X-ray absorption fine structure (EXAFS). These analyses have provided abundant information about cation

* E-mail: javc@nhm.ac.uk
DOI: 10.1180/0009855023730046

ordering in the octahedral sheet, *cis-trans* occupancy and layer stacking (Dainyak *et al.*, 1992; Schroeder, 1993; McCarty and Reynolds, 1995, 2001; Drits *et al.*, 1997; Muller *et al.*, 1997; Cuadros and Altaner, 1998; Cuadros *et al.*, 1999; Manceau *et al.*, 2000). This information helps to provide an understanding of the processes of smectite illitization in different environments, as well as the mechanisms of stabilization of the mineral phases involved in the reaction. Hence, these studies have helped to reveal a more complete picture of smectite from which chemical composition can be related to crystal structure and crystal defect information. In the near future it will be possible to correlate composition and structural factors and then to interpret these correlations in terms of smectite stability. Conversely, we will also be able to understand why these correlations are not applicable in every case and how they are affected by original rock type and composition, different mechanisms of smectite crystallization (depending on alteration conditions), kinetics of smectite formation, etc.

This paper reports and interprets the study of some smectites of different compositions that have been submitted to Cs exchange and wetting-and-drying cycles. This study is combined with previous analyses from the literature to highlight some of the crystal-chemical features of smectite.

MATERIALS AND METHODS

Smectites

Six smectite samples were selected for analysis: the montmorillonites SAz-1 (Arizona, USA), Chambers (Arizona, USA), Belle Fourche (South Dakota, USA) and SWy-1 (Wyoming, USA), and two samples of nontronite 33B (Manito County, Washington, USA). One of the two nontronite samples was from the collection at the Estación Experimental del Zaidín (CSIC, Granada, Spain) and will be referred to as 33B EEZ. The other nontronite sample was provided by Peter Komadel (Slovak Academy of Sciences, Bratislava, Slovakia) and is termed 33B Sk. The montmorillonites were also from the collection at Estación Experimental del Zaidín. These smectites were selected because of their different chemical compositions (see below). The difficulty in obtaining nontronite from different localities led to the use of two samples from the same locality, probably collected at different times and from different exposures. Beidellite SBID-1 (Idaho, USA) was initially considered for inclusion in this study, but was found to contain halloysite and was then discarded. The smectites were centrifuged and the <2 μm size fraction was collected and used in the subsequent analyses. Initial characterization of these samples was performed by XRD of oriented mounts. The mounts were prepared by dispersion in deionized water, placing a few drops of the dispersion onto glass slides and allowing them to dry. The mounts were glycolated by placing them in a glycol-saturated atmosphere at 60°C overnight. The XRD analysis was performed in a Philips PW 1710 with a Cu anode, graphite monochromator, 1° divergence slit and 0.2 mm receiving slit, at 40 kV, 40 mA, 0.05°2θ step size and 2 s step count. The patterns showed that the samples are smectite with no mixed-layer component or any other clay mineral phase (although XRD of the powder samples showed the presence of trace amounts of other minerals; see below).

The Chambers, Belle Fourche and 33B EEZ smectites were analysed chemically by X-ray fluorescence (XRF) and SWy-1 by wet analysis. The composition of 33B Sk was taken from Čičel and Machajdík (1981). The XRF was performed using a Philips PW 1404 spectrometer after diluting (1:10 in $Li_2B_4O_7$) and fusing the samples. In the wet chemical analysis Si, Al and Fe were analysed by spectrophotometry, using the molybdate blue, alizarin red-S and orthophenanthroline methods, respectively (Shapiro, 1975); Ca and Mg were determined by atomic absorption, and Na and K by flame emission spectroscopy. The chemical compositions were transformed into structural formulae (Table 1). Initially, an octahedral occupancy >2 resulted for SAz-1 and SWy-1. For these two samples, the interlayer Mg was analysed to discriminate between octahedral and interlayer Mg. Interlayer cations were displaced by exchanging twice with a 1.5 M $CaCl_2$ solution. The resulting solution was analysed for Mg by atomic absorption and the corresponding amount was assigned to the smectite interlayer.

Sample preparation and analysis

Prior to treatment, the samples were analysed by differential thermal analysis (DTA) and thermogravimetry (TG) using a Netzsch STA 409 EP, at 10°C/min, with Al_2O_3 as the reference, in Al_2O_3

TABLE 1. Structural formulae per half formula unit.

	Si^{IV}	Al^{IV}	Al^{VI}	Fe^{3+VI}	Mg^{VI}	Mn^{VI}	Ti^{VI}	Na	K	Ca	Mg^{int}	Σ Oct
SAz-1	3.99	0.01	1.38	0.07	0.53	0.00	0.01	0.04	0.01	0.20	0.03	1.99
Chambers	3.86	0.14	1.37	0.18	0.41	0.00	0.02	0.02	0.00	0.28		1.98
Belle Fourche	3.96	0.04	1.56	0.17	0.25	0.00	0.01	0.25	0.01	0.03		1.99
33B EEZ	3.46	0.54	0.19	1.77	0.06	0.01	0.03	0.00	0.00	0.17	0.04	2.06
33B Sk[1]	3.49	0.51	0.15	1.80	0.02					0.32		1.97
SWy-1	3.98	0.02	1.44	0.22	0.30	n.d.	n.d.	0.44				1.96

[1] From Čičel and Machajdík (1981)
n.d.: not determined

crucibles. 0.5 g aliquots of the samples were Li-exchanged twice with a 0.25 N LiCl solution, to ensure complete dispersion, and then Cs-exchanged using 0.25 N CsCl. The samples were washed with deionized water by centrifugation until no Cl^- was detected with the $AgNO_3$ method. The smectites were then submitted to 70 wetting-and-drying cycles, using deionized water and drying in an oven at 60°C. Previous wetting-and-drying experiments have shown that after 40–60 cycles, the increase of collapsed layers is very small (Eberl *et al.*, 1986; Šucha and Širáňová, 1991). The cycles were carried out in 6 cm diameter tubes that allowed a large contact surface between smectite and water. When adding water, the tubes were stirred gently to ensure that all smectite was soaked, but without causing dispersion of the aggregates formed. After the cycles, the aggregates (scales of different lateral dimensions and thicknesses) were cut repeatedly (not ground) with a sharp blade until they had a powder appearance.

The powdered samples were prepared as oriented, glycolated mounts using the procedure described above. Dispersion in water for the mount preparation was very gentle to avoid disruption of the layer stacking attained during the wetting and drying cycles. For this reason the films were rough (low degree of preferred orientation) except in the case of Belle Fourche and SWy-1. Powder XRD was performed in a machine with the same characteristics as those previously described, except that the receiving slit was set at 0.1 mm and that it was equipped with a high-temperature and vacuum chamber. The sample was fixed to a flat platinum bar sample holder (with an attached thermopar) by spreading a thin layer of vaseline on the holder, placing a small amount of the sample on it, ensuring a uniform, thin layer, and pressing the sample very gently with a spatula edge to ensure adherence while trying to avoid particle orientation. Vaseline has a very broad and weak XRD signal that did not interfere with the smectite patterns. The chamber was evacuated to 5.3×10^{-3} – 7×10^{-3} mbar (taking ~15 min), then the temperature was increased to 200°C (taking 3 min); there was a wait of 10 min, and then the sample was scanned between 19 and 44°2θ, with a step size of 0.04°2θ and step count of 90 s. With this procedure, complete dehydration of smectite was attained, which helped to maintain a fixed *d*-spacing and improve the quality of three-dimensional patterns.

The XRD patterns of the glycolated mounts (after wetting and drying) were simulated using NEWMOD (Reynolds, 1985). Interlayer Cs (not available in the computer programme) was simulated using K and the following interlayer occupancy: occupancy = determined occupancy × number or electrons in Cs^+/number of electrons in K^+. The powder patterns were also simulated using NEWMOD for the 00*l* series peaks and WILDFIRE (Reynolds, 1993) for the *hkl* reflections. The experimental powder patterns showed different degrees of preferred orientation (different relative intensities of 00*l* *vs.* *hkl* peaks), hence the simulated 00*l* and *hkl* patterns were mixed in adequate proportions to match the experimental traces. The files with the atomic coordinates for the simulation of *hkl* reflections were modified to account for the presence of Cs instead of K by using a c^* dimension of 11 Å, as observed in the experimental patterns, and moving the interlayer cation from 0.5 to 0.55 normalized distance from the octahedral cation plane (representing the origin for the c^* direction coordinate). The latter is to locate the cation in the centre of the now larger interlayer. The interlayer occupancy was initially calculated

with the equation defined above, although in most cases this value was later changed to provide a better match to the experimental patterns (see below). Further information about the calculations is provided in the appendix.

RESULTS

The XRD analysis of the oriented, glycolated smectites revealed different proportions of collapsed layers after the wetting-and-drying cycles (Fig. 1, Table 2). Layer collapse is dependent on layer charge and charge location (Eberl *et al*., 1986; Šucha and Širáňová, 1991). The two 33B samples have the greatest proportions of collapsed layers, which is consistent with their high tetrahedral charge (Table 1) which favours attraction between interlayer Cs and layers. The lowest proportions of non-expandable layers correspond to Belle Fourche and SWy-1, which have low tetrahedral charge and relatively low layer charge. On the other hand, charge may not be the only cause of the greater degree of layer collapse. Particle shape and size may also play a role and small, equidimensional particles may rotate more easily during the wetting-and-drying cycles attaining an orientation in which hexagonal rings exist directly across the interlayer and Cs ions occupy the resulting cavities (the six-fold rings created by the tetrahedra are referred to here as 'hexagonal' irrespective of their actual shape owing to tetrahedron rotation). Belle Fourche and SWy-1 dispersed better in water during preparation of the oriented aggregates and were much better oriented than the other samples, which resulted in more intense 00*l* peaks. The collapsed layers have a *d*-spacing of 11 Å. Some of the peaks in the simulations are slightly displaced, perhaps indicating the presence of a few layers with a spacing intermediate between 2-glycol layers (16.9 Å) and fully collapsed (11 Å).

Thermal analysis showed the temperatures of dehydroxylation. Dehydroxylation events are marked with a vertical line in Fig. 2. It is now well established that dioctahedral *trans*-vacant layers of 2:1 phyllosilicates dehydroxylate between 500 and 600°C, while *cis*-vacant ones do

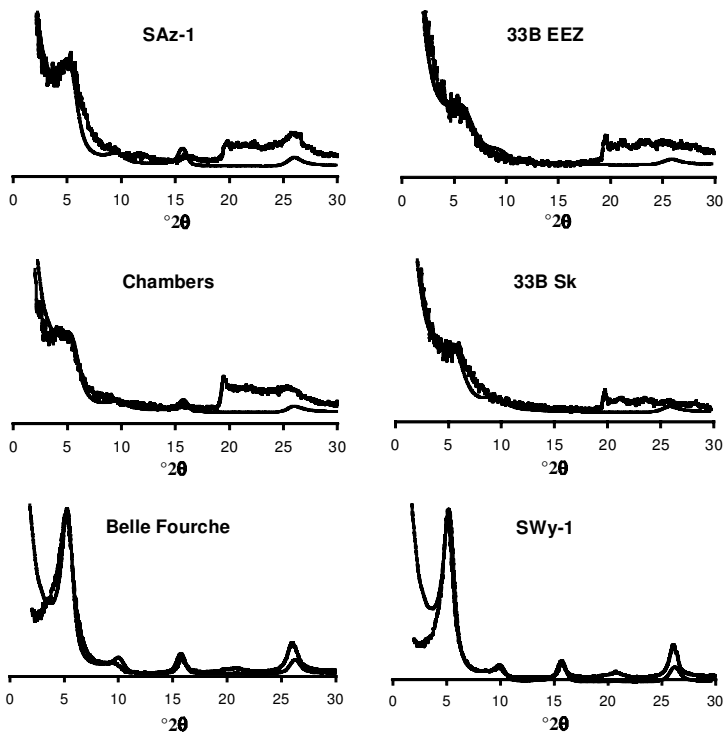

FIG. 1. Experimental XRD patterns and simulations of the oriented and glycolated specimens after Cs-exchange and wetting and drying.

TABLE 2. Percentage of non-expandable layers, as determined from glycolated mounts, and parameters used in the calculations of powder XRD patterns.

	Glycol	Powder				
	% non-expandable	Interlayer occupancy Experimental[1]	Calculated[2]	% 3-D coherent[3]	P^4_{cv}	P^5_0
SAz-1	40	1.53	1.3	40	0.9	1
Chambers	45	1.77	1.1	25	0.9	1
Belle Fourche	20	0.96	0.96	20	1	1
33B EEZ	60	1.28	1.9	40	0	1
33B Sk	55	1.92	1.9	40	0	1
SWy-1	15	1.32	1	15	1	1

[1] From chemical analysis, using the formula occupancy = determined occupancy × number of electrons in Cs^+/number of electrons in K^+
[2] Best match with experimental patterns
[3] Percent of 3-dimensionally coherent layers
[4] Fraction of *cis*-vacant layers
[5] Fraction of non-rotated layers

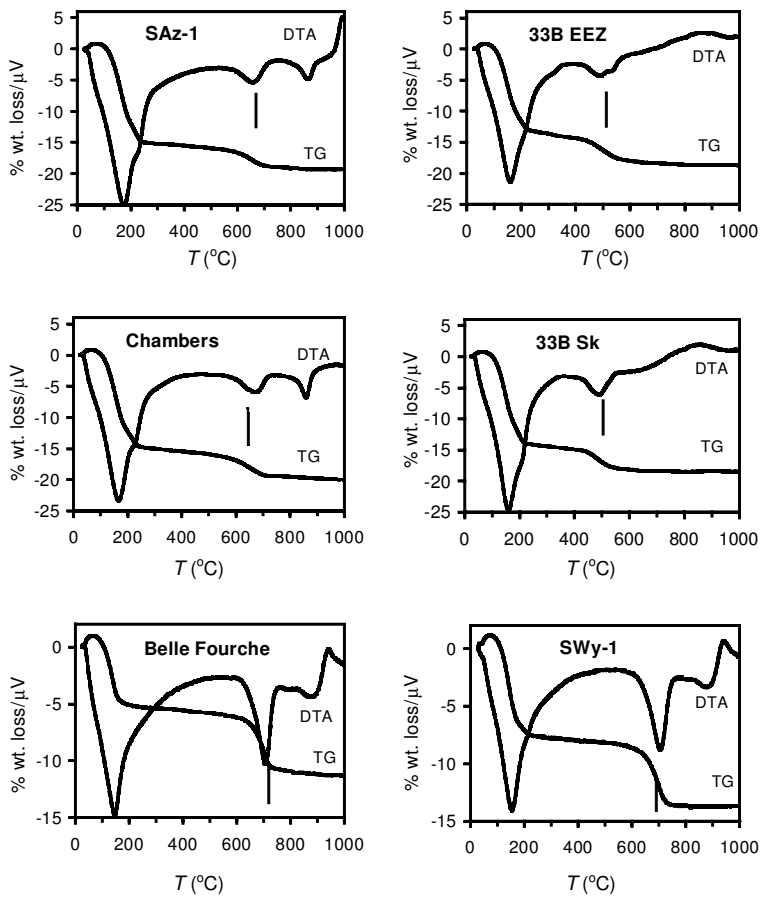

FIG. 2. DTA and TG traces of the smectites, performed prior to Cs-exchange. The vertical line in the plot indicates the dehydroxylation event.

so at 600–700°C (Drits *et al.*, 1995; Cuadros and Altaner, 1998; Drits *et al.*, 1998; Muller *et al.*, 2000). Accordingly, the two 33B samples are *trans*-vacant and the others are *cis*-vacant. Interestingly, 33B EEZ presents two dehydroxylation minima in the DTA trace whereas 33B Sk shows only one. This indicates that they are not identical, even though their tetrahedral and octahedral compositions are very similar. The small initial increase in the TG lines corresponds to the buoyancy effect produced by heating, that remained uncorrected.

The powder XRD patterns and the corresponding simulations are shown in Fig. 3, and the parameters used in the calculations are in Table 2. Samples 33B EEZ and 33B Sk have very similar patterns and only the former was simulated, although the corresponding simulation parameters are shown in Table 2 for both. Belle Fourche and SWy-1 patterns are dominated by the one-dimensional 00*l* series (intense peaks at 24.5 and 32.4°2θ, and a low-intensity component of the peak at 40.5°2θ, corresponding to 003, 004 and 005, respectively). This indicates that these samples are affected by preferred orientation, possibly due to their particle morphology, although no difference between these and the other smectites was observed while placed on the heating stage. The calculated patterns were appreciably affected by the amount of interlayer Cs because Cs^+ has a large number of electrons. For each smectite, larger amounts of Cs decreased the intensity of the 020, 110 reflection (20°2θ). Observation of the absolute intensities showed that, in fact, higher amounts of Cs increase the intensity of all reflections except 020, 110. Initially, the amount of interlayer Cs used in the simulations was calculated with the equation at the foot of Table 2, using the chemical analysis results (third column in Table 2). However, except for Belle Fourche and 33B Sk, the simulations had 020, 110 reflections with incorrect relative intensities and thus Cs amounts were varied to make the experimental and modelled intensities fit (fourth column in Table 2). The causes for these differences are discussed below.

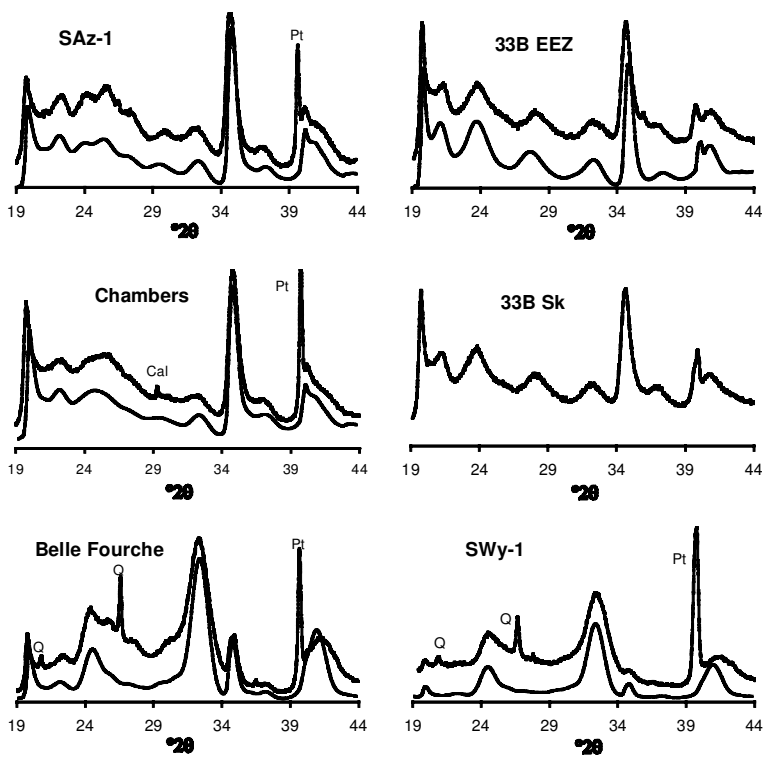

FIG. 3. Experimental X-ray patterns and simulations of the powder smectite samples after Cs-exchange and wetting and drying. Cal: calcite; Q: quartz; Pt: platinum reflection from the sample holder.

The best-fit parameters from the simulations are shown in Table 2. For SAz-1, Belle Fourche and SWy-1 the proportion of layers stacked coherently is the same, within error, as the proportion of non-expandable layers (determined from the glycolated mounts). For Chambers and the two 33B samples, the proportion of coherently stacked layers is smaller, meaning that some non-expandable layers are rotated randomly with respect to each other by any angle different from 60° or a multiple of this. These random rotations destroy diffraction coherence across layers. The determination of both magnitudes, expandable and 3-dimensional coherent layer proportion, is affected by the uncertainty emerging from the fact that a range of values can generate undifferentiated patterns. For expandability the error is considered to be ~10% (Moore & Reynolds, 1997). For the proportion of coherent layers, the error depends upon the degree of order of the calculated structure. More ordered structures are more sensitive to parameter variations. Calculations with the present structures show an error range from 15%, for Chambers, to 10%, for 33B. For Belle Fourche and SWy-1 the error is probably larger. Interestingly, there is complete absence of rotation in the 3-dimensionally coherent layers (P_0 parameter). Hence, within the quoted error range, SAz-1, Belle Fourche and SWy-1 can be considered as consisting of turbostratically-stacked layers which expand upon glycolation and non-expandable, 1*M*-type layers. Chambers and the two 33B smectites also have non-expandable, randomly rotated layers. Finally, SAz-1, Belle Fourche and SWy-1 are *cis*-vacant (P_{cv}), SAz-1 and Chambers are almost entirely so, and the two 33B samples are *trans*-vacant. This is in total agreement with the DTA-TG results.

DISCUSSION

Layer rotation

According to Besson *et al.* (1983), collapsed smectite layers with interlayer Cs can have two *d*-spacings, 10.8 Å if all the Cs ions are located in the cavities created by facing hexagonal rings in the tetrahedral sheet, and 11.6 Å if the hexagonal rings are not directly opposing each other and thus the cavities are half the size. The collapsed layers in this study have a *d*-spacing of 11 Å, measured using the 00*l* reflections in the powder samples, in a completely dehydrated state. Also, this value allowed successful modelling of the patterns for the oriented, glycolated specimens. Such a basal spacing indicates that in the majority (at least 75%), if not all of the layers, Cs occupies the cavity created by facing hexagonal rings. This must evidently be the case for the 1*M*-type layers found in all the samples. For the randomly rotated layers (whether they are expandable with the glycol treatment or not) the situation must be explored in more detail because layer rotation decreases the number of cavities as many of the hexagonal rings cease to confront a counterpart in the adjacent layer. We need to assess whether the rotated layers have enough hexagonal cavities to house all Cs atoms and, hence, can develop the experimentally measured spacing of 11 Å. Guthrie & Reynolds (1998) addressed this problem, showing how layer rotation creates patterns of zones where cavities exist (with different overlapping areas between the hexagonal rings in the two layers) separated by zones where they do not (Fig. 4). The patterns have a hexagonal symmetry following the shape of the hexagonal rings. We are only concerned with random rotations, excluding any multiple of 60° (which would be detected as coherent layer stacking). For the analysis of the available cavities, only the symmetry of the patterns created by rotation applies, not the crystallographic symmetry of the layers, hence, only rotations between 0° and 30° need to be considered. The greater the angle of rotation, the smaller the size of the patterns and the more numerous. These patterns follow the equation:

$$D \supset \frac{d_1}{2 \sin \frac{\beta}{2}}$$

where D is the dimension of the bidimensional lattice created by the patterns (distance between the centres of the patterns), d_1 is the dimension of the original lattice creating these patterns by rotation (distance between the centres of hexagonal rings), and β is the angle of rotation between layers.

Considering the interlayer space (11 Å), the dimensions of the hexagonal ring (5.2 Å vertex to vertex, 4.6 Å side to side) and the radii of Cs^+ (1.7 Å) and O^{2-} (1.26 Å), the Cs ion fits very tightly in the cavity. If the hexagonal rings are not exactly confronted, no Cs ion can be located in the corresponding cavity. Hence, only the central spot of every pattern, where hexagonal rings confront each other exactly, will permit the location of Cs. The proportion of available rings for Cs can be

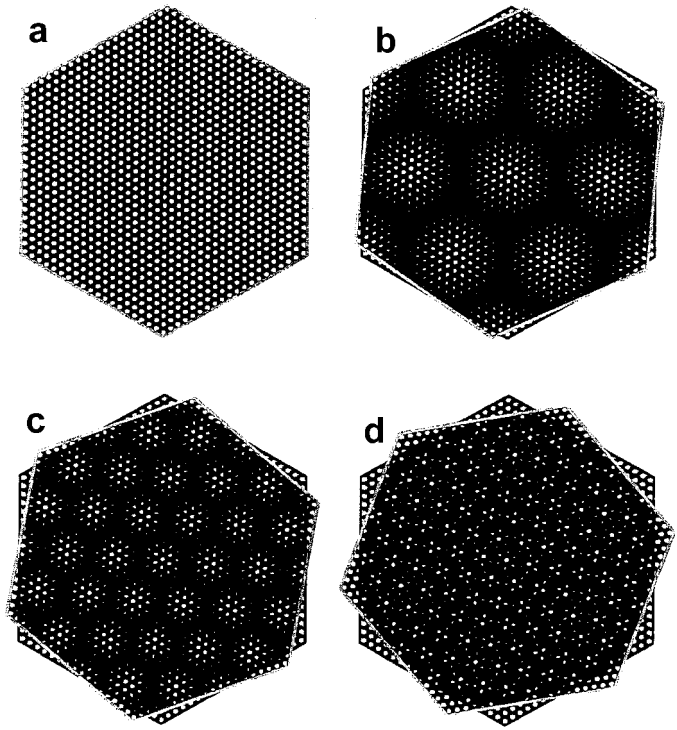

FIG. 4. Pattern development produced by the hexagonal rings as two consecutive layers are rotated (reproduced, with permission, from Guthrie and Reynolds, 1998).

assessed in the following way. Consider two ideal hexagonal layers (as depicted in Fig. 4), with a side-to-side diameter of 600 Å. The total number of hexagonal rings in each layer can be calculated as area of layer/area of hexagonal ring (the area of the hexagonal ring includes the contribution of the basal faces of the tetrahedra, which also occupy part of the layer area). The area of the rotation patterns can be calculated from the distance between the centres of the patterns (D in the equation above), which is equivalent to their side-to-side diameters. With this information we can calculate the total number of rotational patterns as area of the layer/area of the pattern. Considering that there is only one usable site per rotational pattern, we can finally calculate the proportion of usable sites with respect to the number of hexagonal rings in one layer, at different angles (Table 3). This number increases with the number of patterns, i.e. with increasing rotational angles.

The interlayer occupancies (number of Cs ions per hexagonal ring) determined by chemical analysis or by the WILDFIRE calculations are greater than the number of sites available even for the most favourable case (Table 3, 28%). According to this, the number of Cs ions that can be located between randomly rotated layers is insufficient to account for the total interlayer Cs. A possible explanation is that the excess Cs is located in external hexagonal rings. Figure 4d shows that the rotation of layers leaves the vertices of the ideal hexagonal layers exposed. If the exposed hexagonal rings of the internal sides of both layers are considered, the number of available sites increases, such that for a 30° rotation the proportion of available sites is 40% (Table 3). In reality, smectite layers do not have such regular shapes and there is a variety of particle sizes, hence stacking will probably create many zones of exposed surfaces and the contribution of these areas to Cs allocation must be high. This distribution of Cs is not homogeneous, with more Cs ions in the exposed external areas than in the interlayers. This inhomogeneity can be minimized if the layers have a small surface. Stacking randomly-rotated small layers will create exposed surfaces randomly

TABLE 3. Angle of rotation between layers and resulting proportion of interlayer cavities that can contain a Cs ion, and interlayer occupancy from chemical data and WILDFIRE calculations.

Angle (°)	% usable sites		% interlayer occupancy	
			Chemical analysis	WILDFIRE
1	0			
5	1	SAz-1	51	43
10	3	Chambers	59	37
15	7	Belle Fourche	32	32
20	13	33B EEZ	43	63
25	20	33B Sk	64	nc
30	28 (40)[1]	SWy-1	44	33

[1] Value in parenthesis calculated using the non-overlapping areas (see text)
nc: Not calculated

distributed in the borders as well as in central areas, thus generating small regions of higher and lower Cs concentration. Also, it is possible for a layer to frequently have an exposed area on one side and an interlayer area on the other, so that the layer charge is locally balanced. Large-surface layers will tend to have large contact areas and the inhomogeneous distribution of Cs would be more marked. Larger areas of both high and low Cs concentration are less likely because charge balance becomes less favoured. This interpretation is in agreement with the finding of Besson *et al.* (1983) that Cs-smectite and K-smectite submitted to wetting-and-drying cycles had particles (aggregates of layers) more than one order of magnitude smaller than before the treatment. The existence of external (non-interlayer) Cs is probably the explanation for the discrepancy between interlayer Cs obtained by chemical analysis and calculated by WILDFIRE. Larger amounts of Cs increase the intensity of the patterns except for the 020, 110 reflection because this is the only one without an l component and so is unaffected by Cs. The external Cs does not contribute to the diffracting intensity and the total Cs content appears to be lower than it is. This affects non-rotated layers and randomly rotated layers, since the intensity of both the pattern background (randomly rotated layers) and of the peaks (non-rotated layers) is affected. Even though non-rotated layers can accommodate all Cs in the interlayer, the effect is felt due to the small size of the layers and their patchy arrangement created during the wetting-and-drying cycles, that leaves some Cs on the external side of layers. However, 33B EEZ behaves the opposite way, with a calculated Cs greater than the experimentally measured value. In this case, the chemical analysis may have yielded a low interlayer occupancy.

The resulting picture is that Cs exchange and wetting and drying induced some smectite layers to stack without mutual rotation and other layers to stack with random rotations of ~30° or its multiples 90, 150, 210, 270 and 330°. Angles diverging from these (except for 60° and multiples, where coherent stacking exists) will not permit incorporation of all Cs atoms. This seems to indicate that the smectite layers were rotated in all possible angles before Cs exchange, as might be expected because they had previously been Li-exchanged, which causes complete disruption of the original smectite crystallites. The Cs exchange and wetting and drying causes the layers to rotate to whichever of the above angles is closer in order to have an energetically favourable disposition. This process is accompanied by a reduction of the layer size that facilitates it. It is interesting to note that no rotations of 120, 240 or 60, 180 or 300° were detected. Tsipursky & Drits (1983) obtained a similar result with K-exchange and 70–100 wetting-and-drying cycles, although they calculated that up to 30% of layers rotated by 120° could be present. In this study no uncertainty was calculated for the parameter P_0 (proportion of non-rotated layers), although the patterns were appreciably different when it was made 10% lower. An alternative result was obtained by Grathoff and Eisenhour (1998), who found about 50% of non-rotated layers with K-exchange and 50 cycles of wetting and drying. In the present study, not only the non-rotated layers became non-expandable (as tested with glycol) but also some of the randomly rotated layers in Chambers and the two 33B

samples. This is an unexpected result and indicates that the layer arrangement can be attained in such a way that the inhomogeneous Cs distribution does not create an energy barrier that impedes the existence of stable collapsed layers. Finally, all layers were collapsed (11 Å) after vacuum and heating at 200°C, although it is not known whether all of them are non-expandable when exposed to glycol. The redistribution of the interlayer Cs during layer arrangement requires an import of energy. In the case of layers that collapsed during the wetting-and-drying cycles (with random rotations) the many cycles and the aqueous phase provide a long time-span and an appropriate environment for Cs redistribution. In the case of those that collapsed while dehydrated at 200°C the high temperature could provide the required energy.

Chemical composition, lateral sheet dimension and cis-trans occupancy

The chemical compositions of the studied smectites (Table 1) show a marked increase in tetrahedral substitution in the two nontronite samples (33B) over the others. In fact, for low-temperature smectites, a positive correlation between octahedral Fe^{3+} and tetrahedral Al has been recognized (Tardy *et al*., 1987). In principle, two factors could be invoked for such a correlation, namely electrical charge and cation size.

TABLE 4. Literature references for the smectites used to calculate the ideal tetrahedral and octahedral *b* parameters, and the calculated values (in Å).

Bentonites	Type*	Reference		b_{oct}	b_{tet}
Ascan	Montmorillonite	Tsipursky & Drits (1984)	n. 1**	8.42	9.29
Ascan	Beidellite	"	n. 12	8.35	9.33
Gumbrin		"	n.7	8.43	9.28
Oglanlyn		"	n. 5	8.39	9.28
Sarygiukh		"	n. 8	8.41	9.28
JP	Montmorillonite	Madejová *et al*. (1994)		8.38	9.30
Garfield	Nontronite	Bonnin *et al*. (1985)		8.68	9.37
Garfield	"	Manceau *et al*. (2000)		8.64	9.35
SWa-1	"	"		8.57	9.33
Stebno		Čičel *et al*. (1992)		8.50	9.35
Gammano		Weaver & Pollard (1973)		8.44	9.32
SM16		Christidis & Dunham (1993)		8.40	9.31
SM25		"		8.39	9.30
SM43		"		8.39	9.31
SM66		"		8.36	9.31
SM99		"		8.39	9.29
SM114		"		8.42	9.29
SM119		"		8.39	9.29
SM228		"		8.42	9.30
93-6-8c		Ylagan *et al*. (2000)		8.40	9.28
Non-bentonites					
Weathering of gneisses		Tsipursky & Drits (1984)	n. 17	8.61	9.38
Kazakhstan	Soil	"	n. 9	8.39	9.31
Pacific Ocean		"	n. 16	8.51	9.36
Uterrupsroth	Beidellite	Besson & Tchoubar (1972)		8.32	9.36
Panamint Valley	Nontronite	Manceau *et al*. (2000)		8.64	9.35
Houston		Sposito (1986)		8.41	9.33
Missouri	Beidellite	"		8.41	9.36
Salobo		Petit *et al*. (1992)		8.69	9.35

* Type where identified in the original work.
** These numbers refer to those given in the paper by Tsipursky & Drits (1984).

Nevertheless, while both are present in the Al:Si substitution on the tetrahedral sites, there are only size effects and not charge effects implicated in the Fe:Al substitution on octahedral sites. For this reason, the size effects were investigated. Considering the ideal tetrahedral and octahedral sheets, without the distortions produced by tetrahedral-octahedral mismatch or other reason, the ideal tetrahedral and octahedral *b* dimensions can be calculated as follows, *b* tetrahedral = $4\sqrt{2}d_{t-o}$, *b* octahedral = $3\sqrt{2}d_{m-o}$, where d_{t-o} and d_{m-o} represent the mean tetrahedral cation- and octahedral cation-oxygen distances, respectively. These distances can be calculated from the chemical composition of the smectite and the radii of both the O^{2-} and the cations in tetrahedral and octahedral coordinations. This calculation was performed for the smectites analysed in this work and others taken from the literature, most of which are from bentonites (Table 4). Figure 5 shows that the ideal *b* parameters of the octahedral and tetrahedral sheets correlate well, indicating that an increase of tetrahedral Al causes an increase of octahedral Fe+Mg, or *vice versa*. The uncertainty in the determination of the parameters, calculated from typical analytical errors, is represented in one of the data points. This uncertainty should only be considered as an assessment because the techniques and dates of analysis are different. The values from bentonites correlate better than those from other smectite samples. This is probably because the latter are less pure and the chemical data are thus affected by other mineral phases. Two regressions are calculated in Fig. 4, one with the samples from this study and one with all bentonites. The corresponding lines are almost coincident, although R^2 is lower for the group of all bentonites.

These results show that although the octahedral sheet flattens and the tetrahedral sheets rotate and tilt in different degrees to match each other, a lateral growth of the dimension of one sheet due to chemical composition causes a chemically-induced growth in the other. This mechanism of stabilization operates in low-temperature smectites but not in smectites precipitated at high temperature or in other 2:1 phyllosilicates characteristic of higher temperatures as illite and dioctahedral micas frequently have high tetrahedral substitutions and low octahedral Mg+Fe. This is also evident in hydrothermal celadonite and nontronite, where the octahedral Fe correlates negatively with the tetrahedral Al (Tardy *et al.*, 1987). Beidellite also falls out of this trend because it has a high Al content both in the tetrahedral and octahedral

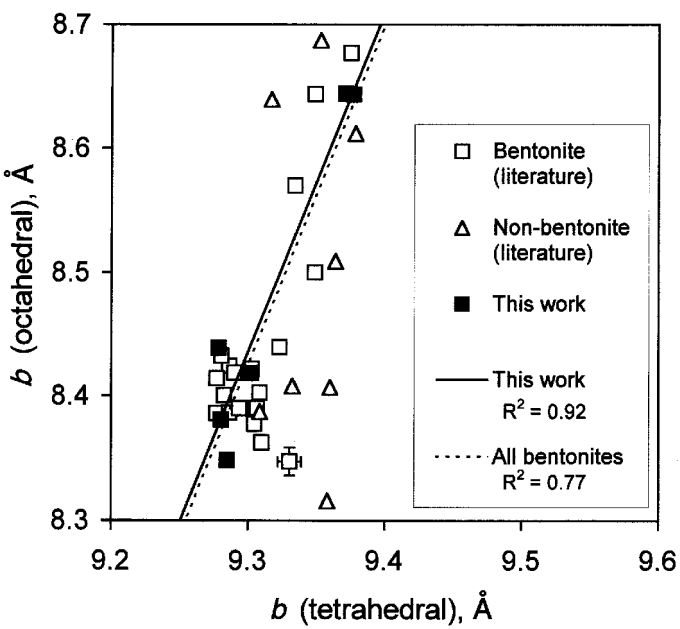

FIG. 5. Plot of the ideal *b* dimensions of the tetrahedral and octahedral sheets of smectites, calculated from their chemical composition.

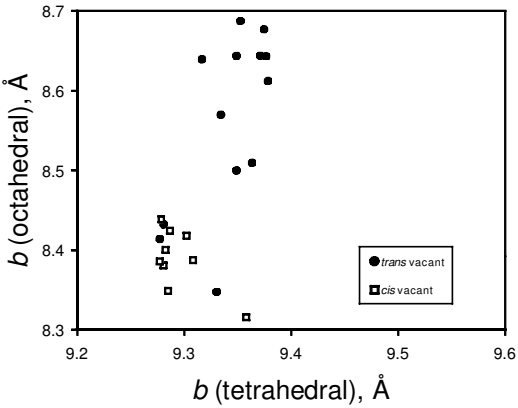

FIG. 6. *Cis*- and *trans*-vacant character of smectites in relation to their ideal tetrahedral and octahedral *b* dimensions.

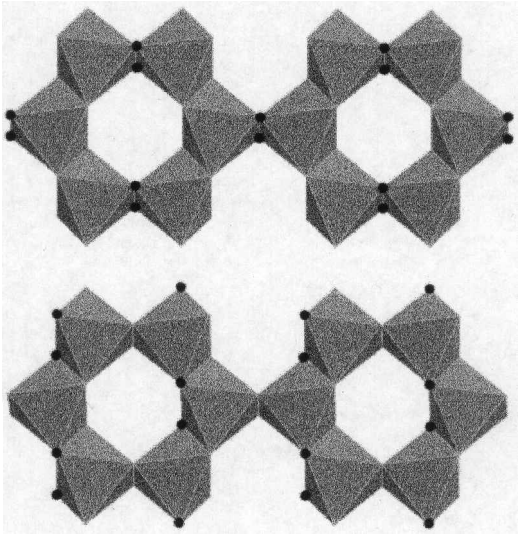

FIG. 7. Octahedral sheets showing the location of hydroxyls (dots) in a *trans*-vacant (upper) and *cis*-vacant (lower) sheet.

sheets. The three beidellites in Fig. 5 plot in the lower right-hand side, at the *b* tetrahedral, *b* octahedral values of 9.36, 8.41 (Missouri, triangle), 9.35, 8.31 (Uterrupsroth, triangle) and 9.33, 8.35 (Ascan n. 12, square). This difference may indeed explain why beidellite is so rare.

The *trans*- and *cis*-vacant character of the smectites in Table 4 and Fig. 5 is represented in Fig. 6 (for 93-6-8c this information is in Drits *et al*., 1998). Labels are assigned to those cases for which the structure has been determined to be >75% *trans*- or *cis*-vacant. The occurrence of one or the other type of octahedral arrangement is dependent upon the chemical composition and the corresponding lateral dimensions of the ideal tetrahedral and octahedral sheets. The only exceptions to the separation into two well-delimited fields are Gumbrin (*b* tetrahedral, *b* octahedral: 9.28, 8.43; hardly visible in the plot), Sarygiukh (9.28, 8.41) and the beidellite Ascan n. 12 (9.33, 8.35). Similar to the results of this work, Petit *et al.* (1992) found that Fe is associated with *cis* sites in smectite, so that increasing Fe causes smectite to be increasingly *trans*-vacant. Also, McCarty and Reynolds (1995, 2001) have found the same trend in illite-smectite, with a decreasing *cis*-vacant nature as Fe+Mg increases.

A possible explanation of this behaviour is presented here, based on the effect of the location of hydroxyls on the lateral dimension of the octahedral sheet (Fig. 7). The shared edges of the octahedra are shortened to minimize the repulsion of the cations. In a *trans*-vacant sheet (upper) there are two types of shared edges: (1) those with two hydroxyls; and (2) those with two oxide ions. In the *cis*-vacant sheet there are also two types: (1) those with two oxide ions; and (2) those with one hydroxyl and oxide ion. The edges of type 2 in both structures have a larger effect on the *b* dimension because they have a component in that direction (horizontal direction in Fig. 7). Hence, only the edges of type 2 are considered. Two oxide ions (*trans*-vacant) are more effective in their screening effect than one hydroxyl and one oxide ion (*cis*-vacant). To have the same screening effect, edges of type 2 in *cis*-vacant sheets need to be slightly shorter. In such a scenario, a *cis*-vacant sheet will have a somewhat smaller *b* dimension (*per se*, without considering attachment and fitting with tetrahedral sheets) than a *trans*-vacant sheet. This could be why a *cis*-vacant sheet is preferred when the tetrahedral sheets have a low substitution, with a smaller lateral dimension, and a *trans*-vacant sheet is preferred when the tetrahedral sheets have larger substitution and, hence, are larger.

ACKNOWLEDGMENTS

The financial support was from DGICYT (Spain), project PB97-1215. The wetting-and-drying experiments were carried out at Departamento de Ciencias de

la Tierra y Química Ambiental, Estación Experimental del Zaidín (CSIC), Granada, Spain. The XRD analyses were performed at Instituto de Ciencia de Materiales (CSIC), Madrid, Spain. I thank José Linares for discussion in the early stages of this work, Eladio Vila for help in performing the X-ray experiments and Paul Schofield and two anonymous reviewers for their helpful comments on the manuscript.

REFERENCES

Besson G. & Tchoubar C. (1972) Determination du group de symmetry du feuillet elementaire de la beidellite. *Comptes Rendus de l'Academie des Sciences de Paris*, **275**, 633–636.

Besson G., Glaeser R. & Tchoubar C. (1983) Le cesium, revelateur de structure des smectites. *Clay Minerals*, **18**, 11–19.

Bonnin D., Calas G., Suquet H. & Pezerat H. (1985) Site occupancy of Fe^{3+} in Garfield nontronite. A spectroscopy study. *Physics and Chemistry of Minerals*, **12**, 55–64.

Christidis G. & Dunham A.C. (1993) Compositional variations in smectites: Part I. Alteration of intermediate volcanic rocks. A case study from Milos island, Greece. *Clay Minerals*, **28**, 255–273.

Čičel B. & Machajdík D. (1981) Potassium- and ammonium-treated montmorillonites. I. Interstratified structures with ethylene glycol and water. *Clays and Clay Minerals*, **29**, 40–46.

Čičel B., Komadel P., Lego L., Madejová J. & Vlčková L. (1992) Iron-rich beidellite in the fine fraction of Stebno bentonite. *Geologica Carpathica – Series Clays*, **2**, 121–124.

Cuadros J. & Altaner S.P. (1998) Compositional and structural features of the octahedral sheet in mixed-layer illite/smectite from bentonites. *European Journal of Mineralogy*, **10**, 111–124.

Cuadros J., Sainz-Díaz C.I., Ramírez R. & Hernández-Laguna A. (1999) Analysis of Fe segregation in the octahedral sheet of bentonitic illite-smectite by means of FTIR, ^{27}Al MAS NMR and reverse Monte Carlo simulations. *American Journal of Science*, **299**, 289–308.

Dainyak L.G., Drits V.A. & Heifits L.M. (1992) Computer simulation of cation distribution in dioctahedral 2:1 layer silicates using IR-data: application to Mössbauer spectroscopy of a glauconite sample. *Clays and Clay Minerals*, **40**, 470–479.

Drits V.A., Plançon A., Sakharov B.A., Besson G., Tsipursky S.I. & Tchoubar C. (1984) Diffraction effects calculated for structural models of K-saturated montmorillonite containing different types of defects. *Clay Minerals*, **23**, 541–561.

Drits V.A., Besson G. & Muller F. (1995) An improved model for structural transformations of heat-treated aluminous dioctahedral 2:1 layer silicates. *Clays and Clay Minerals*, **43**, 718–731.

Drits V.A., Dainyak L.G., Muller F., Besson G. & Manceau A. (1997) Isomorphous cation distribution in celadonites, glauconites and Fe-illites determined by infrared, Mössbauer and EXAFS spectroscopies. *Clay Minerals*, **32**, 153–179.

Drits V.A., Lindgreen H., Salyn A.L., Ylagan R.F. and McCarty D.K. (1998) Semiquantitative determination of trans-vacant and cis-vacant 2:1 layers in illites and illite-smectites by thermal analysis and X-ray diffraction. *American Mineralogist*, **83**, 1188–1198.

Eberl D.D., Środoń J. & Northrop H.R. (1986) Potassium fixation in smectite by wetting and drying. Pp. 296–325 in: *Geochemical Processes at Mineral Surfaces* (J.A. Davis & K.F. Hayes, editors). ACS Symposium Series **323**. American Chemical Society, Washington, D.C.

Grathoff G.H. & Eisenhour D.D. (1998) Random powder XRD analysis of seven commercial K-saturated wetted and dried smectites. *Proceedings of the 35th Clay Minerals Society Meeting, Cleveland, Ohio, p.* 67.

Guthrie G.D. Jr. & Reynolds R.C. Jr. (1998) A coherent TEM- and XRD-description of mixed-layer illite/smectite. *The Canadian Mineralogist*, **36**, 1421–1434.

Madejová J., Komadel P. & Čičel B. (1994) Infrared study of octahedral site populations in smectites. *Clay Minerals*, **29**, 319–326.

Manceau, A., Lanson B., Drits V.A., Chateigner D., Gates W.P., Wu J., Huo D. & Stucki J.W. (2000) Oxidation-reduction mechanism of iron in dioctahedral smectites: I. Crystal chemistry of oxidized reference nontronites. *American Mineralogist*, **85**, 133–152.

McCarty D.K. & Reynolds R.C. Jr. (1995) Rotationally disordered illite/smectite in Paleozoic K-bentonites. *Clays and Clay Minerals*, **43**, 271–284.

McCarty D.K. & Reynolds R.C. Jr. (2001) Three-dimensional crystal structures of illite-smectite minerals in Paleozoic K-bentonites from the Appalachian basin. *Clays and Clay Minerals*, **49**, 24–35.

Moore D.M. & Reynolds R.C. Jr. (1997) *X-ray Diffraction and the Identification and Analysis of Clay Minerals*, pp. 261–297. Oxford University Press, Oxford, UK.

Muller F., Besson G., Manceau A. & Drits V.A. (1997) Distribution of isomorphous cations within octahedral sheets in montmorillonite from Camp-Bertaux. *Physics and Chemistry of Minerals*, **24**, 159–166.

Muller F., Drits V., Plançon A. & Robert J. (2000) Structural transformation of 2:1 dioctahedral layer silicates during dehydroxylation-rehydroxylation reactions. *Clays and Clay Minerals*, **48**, 572–585.

Petit S., Prot T., Decarreau A., Mosser C. & Toledo-Groke M.C. (1992) Crystallochemical study of a population of particles in smectites from a lateritic weathering profile. *Clays and Clay Minerals*, **40**, 436–445.

Reynolds, R.C. Jr. (1985) *NEWMOD: A computer program for the calculation of one-dimensional diffraction powders of mixed-layer clays*. 8 Brook Rd., Hanover, NH 03755, USA.

Reynolds R.C. Jr. (1993) Three-dimensional X-ray powder diffraction from disordered illite: simulation and interpretation of the diffraction patterns. Pp. 44–78 in: *Computer Applications to X-ray Powder Diffraction Analysis of Clay Minerals* (R.C. Reynolds and J.R. Walker, editors). CMS Workshop Lectures, **5**. Clay Minerals Society, Boulder, Colorado, USA.

Schroeder P.A. (1993) A chemical, XRD, and ^{27}Al MAS NMR investigation of Miocene Gulf coast shales with application to understanding illite/smectite crystal-chemistry. *Clays and Clay Minerals*, **41**, 668–679.

Shapiro L. (1975) *Rapid Analysis of Silicate, Carbonate, and Phosphate Rocks*. US Geological Survey Bulletin **1401**, Washington D.C., 76 pp.

Sposito G. (1986) The polymer model of thermodynamical clay mineral stability. *Clays and Clay Minerals*, **34**, 198–202.

Šucha V. & Širáňová V. (1991) Ammonium and potassium fixation in smectite by wetting and drying. *Clays and Clay Minerals*, **39**, 556–559.

Tardy Y., Duplay J. & Fritz B. (1987) Stability fields of smectites and illites as a function of temperature and chemical composition. Pp. 461–494 in: *Geochemistry and Mineral Formation in the Earth Surface* (R. Rodríguez-Clemente and Y. Tardy, editors). Consejo Superior de Investigaciones Científicas, Madrid, Spain.

Tchoubar C. (1985) Quantitative determination of the fine structural features in clays by modelling of the X-ray diffraction patterns. *Mineralogica et Petrographica Acta*, **29A**, 35–54.

Tsipursky S.I. & Drits V.A. (1983) The distribution of octahedral cations in the 2:1 layers of dioctahedral smectites studied by oblique-texture electron diffraction. *Clay Minerals*, **19**, 177–193.

Weaver C.E. & Pollard L.D. (1973) *The Chemistry of Clay Minerals*. Elsevier, Amsterdam.

Ylagan R.F., Altaner S.P. & Pozzuoli A. (2000) Reaction mechanisms of smectite illitization associated with hydrothermal alteration from Ponza island, Italy. *Clays and Clay Minerals*, **48**, 610–631.

APPENDIX

TABLE 5. Dimensions of the coherent scattering domains used in the XRD simulations.

	00*l* series†			Powder				
	Min. *N*‡ *c**	Max. *N* *c**	Aver. *N* *c**	Aver. *N* *a*	Aver. *N* *b*	Min. *N* *c**	Max. *N* *c**	Aver. *N* *c**
SAz-1	1	7	5.3	60	30	1	6	1.47
Chambers	1	7	5.3	60	30	1	5	1.25
Belle Fourche	1	7	5.3	60	30	1	4	1.19
33B EEZ#	1	7	5.3	60	30	1	6	1.47
SWy-1	1	7	5.3	60	30	1	4	1.13

† NEWMOD calculations in glycolated and in powder samples
‡ N: number of unit cells in the corresponding crystallographic direction
# 33B Sk was not calculated